

# Deep Active Learning for Multi-Label Classification of Remote Sensing Images

Lars Möllenbrok and Begüm Demir, *Senior Member, IEEE*

**Abstract**—The use of deep neural networks (DNNs) has recently attracted great attention in the framework of the multi-label classification (MLC) of remote sensing (RS) images. To optimize the large number of parameters of DNNs a high number of reliable training images annotated with multi-labels is often required. However, the collection of a large training set is time-consuming, complex and costly. To minimize annotation efforts for data-demanding DNNs, in this paper we present several query functions for active learning (AL) in the context of DNNs for the MLC of RS images. Unlike the AL query functions defined for single-label classification or semantic segmentation problems, each query function presented in this paper is based on the evaluation of two criteria: i) multi-label uncertainty; and ii) multi-label diversity. The multi-label uncertainty criterion is associated to the confidence of the DNNs in correctly assigning multi-labels to each image. To assess the multi-label uncertainty, we present and adapt to the MLC problems three strategies: i) learning multi-label loss ordering; ii) measuring temporal discrepancy of multi-label prediction; and iii) measuring magnitude of approximated gradient embedding. The multi-label diversity criterion aims at selecting a set of uncertain images that are as diverse as possible to reduce the redundancy among them. To assess this criterion we exploit a clustering based strategy. We combine each of the above-mentioned uncertainty strategy with the clustering based diversity strategy, resulting in three different query functions. Experimental results obtained on two benchmark archives show that our query functions result in the selection of a highly informative set of samples at each iteration of the AL process in the context of MLC.

**Index Terms**—Multi-label classification, active learning, multi-label uncertainty, multi-label diversity, deep learning, remote sensing.

## I. INTRODUCTION

THE development of accurate multi-label image scene classification (MLC) methods (which automatically assign multiple land-use land-cover class labels [i.e., multi-labels] to each image scene in an archive) is a growing research interest in remote sensing (RS) [1]. In recent years, deep neural networks (DNNs) have attracted great attention in the MLC of RS images due to their high capability to describe the complex spatial and spectral content of RS images. However, the DNNs need a sufficient number of high-quality (i.e., reliable) training images annotated with multiple class labels. However, the collection of multi-labels is highly costly in terms of human time and effort [2]. To reduce the

annotation effort, active learning (AL) that aims at iteratively expanding the initial labeled training set based on interaction between the user and the classification system can be used. At each AL iteration the most informative unlabeled images (i.e., samples) for a given classifier are selected based on a function (i.e. query function), labeled by a supervisor and added to the current training set. The supervisor is usually a human expert who gives the true class labels to the selected samples. To assess the informativeness of the samples in the context of MLC, the existing AL method in RS is defined in the framework of traditional supervised classifiers (e.g., multi-label support vector machines) [2], relying on hand-crafted features. It exploits a query function based on the evaluation of two criteria: i) multi-label uncertainty; and ii) multi-label diversity. The multi-label uncertainty criterion is associated to the confidence of the MLC algorithm in correctly assigning multi-labels to the considered sample, while the multi-label diversity criterion aims at selecting a set of uncertain samples that are as diverse (distant from one another) as possible, thus reducing the redundancy among the selected uncertain samples. The combination of the two criteria aims to result in the selection of the potentially most informative set of samples at each iteration of the AL process in the context of the considered classifiers. The iterative process is terminated once performance converges or a predefined budget limit is reached. This query function is not suitable to be directly injected in DNNs. To the best of our knowledge, the use of AL in the framework of MLC through DNNs is not investigated yet in RS. Most of the previous AL methods for DNNs are developed for pixel-based classification problems for land-cover maps generation [3], [4]. We would like to note that the development of DL driven AL methods is much more extended in the computer vision community but mainly being focused on the single-label classification or semantic segmentation problems [5]–[9]. In this letter, we take the first step to address this problem and investigate AL query functions that are designed to assess the multi-label uncertainty and multi-label diversity criteria to select the most informative samples at each AL iteration in the framework of DNNs for MLC of RS images.

## II. INVESTIGATED QUERY FUNCTIONS FOR AL IN MLC

Let  $\mathcal{X} = \{\mathbf{X}_1, \dots, \mathbf{X}_N\}$  denote an archive of  $N$  RS images (i.e., samples) and  $\mathbf{X}_n$  be the  $n$ -th image in the archive. We assume that an initial training set  $\mathcal{T}^1$  with  $M$  samples annotated with multi-labels  $\mathcal{Y}^1 = \{\mathbf{y}_1, \dots, \mathbf{y}_M\}$  is available.  $\mathbf{y}_j = [y_1^{(j)}, \dots, y_C^{(j)}] \in \{0, 1\}^C$  is the multi-label vector of image  $\mathbf{X}_j \in \mathcal{T}^1$ , showing which of the  $C$  unique classes

L. Möllenbrok and B. Demir are with the Faculty of Electrical Engineering and Computer Science, Technische Universität Berlin, 10623 Berlin, Germany (emails: l.mollenbrok@tu-berlin.de, demir@tu-berlin.de). This work is supported by the European Research Council (ERC) through the ERC-2017-STG BigEarth Project under Grant 759764 and by the German Ministry for Education and Research as BIFOLD - Berlin Institute for the Foundations of Learning and Data (01IS18025A).

are present, i.e.  $y_c^{(j)} = 1$  is associated to the  $c$ -th class being present and  $y_c^{(j)} = 0$  to the  $c$ -th class being absent, respectively. Each training image is associated with at least one class (i.e. at least one entry is equal to 1). AL aims at iteratively enriching the training set by selecting the most informative samples for the considered DL model from a large unlabeled set of samples. In detail, at every iteration  $\tau$  (starting with  $\tau = 1$ ) the DL model  $\mathcal{F}$  is trained using the training set  $\mathcal{T}^\tau$  and then  $b$  samples are selected from the set  $\mathcal{U}^\tau = \mathcal{X} \setminus \mathcal{T}^\tau$  of unlabeled samples based on a query function that finds the most informative samples for  $\mathcal{F}$ . The value of  $b$  is associated to labeling budget per iteration. The samples selected through the query function are labeled by a human expert and added to the training set to form the enriched training set  $\mathcal{T}^{\tau+1}$  with labels  $\mathcal{Y}^{\tau+1}$ . In this paper, we investigate three AL query functions that are based on the evaluation of two criteria: i) multi-label uncertainty; and ii) multi-label diversity applied in two consecutive steps. In the first step  $m > b$  most uncertain samples are selected, whereas in the second step  $b$  uncertain samples that are diverse are chosen. For training the considered DL model  $\mathcal{F}$  we use binary cross entropy (BCE) loss, which is given by

$$\mathcal{L}_{BCE}(\mathcal{F}(\mathbf{X}_j), \mathbf{y}_j) = - \sum_{i=1}^C y_i^{(j)} \log(p_i^{(j)}) + (1 - y_i^{(j)}) \log(1 - p_i^{(j)}) \quad (1)$$

where  $\mathcal{F}(\mathbf{X}_j) = [p_1^{(j)}, \dots, p_C^{(j)}]$  is the class probability vector outputted by the DL model. In the next sub-sections the strategies for evaluating multi-label uncertainty and multi-label diversity are presented.

#### A. Evaluation of the Multi-Label Uncertainty

The multi-label uncertainty of an unlabeled sample is associated to the model's ability to correctly predict the multi-labels of the considered sample. During training, the samples that the model cannot classify correctly produce higher losses and constitute greater changes of the network parameters. Therefore, samples that are associated to a high loss can be seen as more uncertain (and thus more informative) for the model. To utilise this approach for assessing the uncertainty of an unlabeled sample (for which the true loss cannot be computed directly), estimations of the potential loss can be used. In the following, we present three different strategies to measure the multi-label uncertainty in the framework of DNNs by estimating the loss behaviour for the unlabeled samples.

1) *Learning Multi-Label Loss Ordering (LL)*: Inspired by [7] we use a sub-network to predict a ranking of the multi-label losses of the unlabeled samples. High-ranked samples are assumed to produce a high loss and therefore are considered to be uncertain and selected for annotation. In detail, in addition to the DL model  $\mathcal{F}$  we make use of an auxiliary module  $\mathcal{F}_L$  connected to the DL model. For every training sample  $\mathbf{X}_j$  the hidden features from  $\mathcal{F}$  (which are denoted by  $\mathcal{F}_{hidden}(\mathbf{X}_j)$ ) are fed to  $\mathcal{F}_L$  where they are transformed using global average pooling followed by a fully connected layer with ReLU activation. The transformed features are concatenated and fed

to a last fully connected layer that outputs a prediction value for the multi-label loss ranking  $\hat{l}_j = \mathcal{F}_L(\mathcal{F}_{hidden}(\mathbf{X}_j))$ .  $\mathcal{F}$  and  $\mathcal{F}_L$  are trained jointly. During training, samples are randomly paired within a batch  $B$ . Let  $B^p$  be the set of these pairs. For a pair  $(\mathbf{X}_j, \mathbf{X}_k) \in B^p$  the loss for training  $\mathcal{F}_L$  is given as follows:

$$\mathcal{L}_{\mathcal{F}_L}((l_j, l_k), (\hat{l}_j, \hat{l}_k)) = \max(0, -\text{sign}(l_j - l_k) \cdot (\hat{l}_j - \hat{l}_k) + \xi) \quad (2)$$

where  $l_i = \mathcal{L}_{BCE}(\mathcal{F}(\mathbf{X}_i), \mathbf{y}_i)$  denotes the true loss of a sample  $\mathbf{X}_i$  and  $\xi > 0$  is the margin hyper-parameter. The loss  $\mathcal{L}_{\mathcal{F}_L}$  is high if for a pair the order based on magnitude of the predicted values is reverse to the order of the true losses. By this way, the model learns a relative loss relation between the samples that can be used to rank samples based on their multi-label losses. For a given batch  $B$ , the loss for jointly training the two models is given as:

$$\mathcal{L} = \frac{1}{|B|} \sum_{\mathbf{X}_i \in B} l_i + \lambda \frac{2}{|B|} \sum_{(\mathbf{X}_j, \mathbf{X}_k) \in B^p} \mathcal{L}_{\mathcal{F}_L}((l_j, l_k), (\hat{l}_j, \hat{l}_k)) \quad (3)$$

where  $\lambda$  is a hyper-parameter for controlling the contribution of the multi-label loss prediction sub-network. Once  $\mathcal{F}$  and  $\mathcal{F}_L$  are trained, the uncertainty of an unlabeled sample  $\mathbf{X}_j$  is evaluated as follows:

$$Unc^{LL}(\mathbf{X}_j) = \hat{l}_j. \quad (4)$$

2) *Measuring Temporal Discrepancy of Multi-Label Prediction (TPD)*: In [8] it is shown that the discrepancy of the outputs of the DL model for a sample from two successive AL iterations can be used to estimate the training loss for that sample. The output discrepancy does not depend on the reference label and therefore it can be used to estimate a loss for unlabeled samples. We use this approach to estimate the multi-label loss for the unlabeled samples and use this to assess the uncertainty of a sample. In detail, let  $\mathcal{F}^\tau$  be the DL model obtained after the  $\tau$ -th iteration of the AL process and  $\mathbf{X}_j \in \mathcal{U}^\tau$  be an unlabeled sample. Then, the multi-label uncertainty based on the temporal prediction discrepancy at the  $\tau$ -th iteration is computed as distance:

$$Unc^{TPD}(\mathbf{X}_j) = \|\mathcal{F}^\tau(\mathbf{X}_j) - \mathcal{F}^{\tau-1}(\mathbf{X}_j)\|_2. \quad (5)$$

Note that in the first iteration ( $\tau = 1$ ) no reference model  $\mathcal{F}^{\tau-1}$  is available, which is why we opt for random sampling in this case.

3) *Measuring Magnitude of Approximated Gradient Embeddings (MGE)*: During training, the loss gradients directly effect the update of network parameters. The gradient magnitude determines the extend of the parameter change and thus a large loss gradient can be seen as an indicator of uncertainty. However, the computation of the gradients requires knowledge of the reference labels, which means that gradients for unlabeled samples cannot be computed directly. In [9] it is suggested to use the pseudo-labels as a substitute for the real labels to compute approximations of the gradients, which is shown to constitute a lower bound in terms of the gradient norm. Let  $\hat{\mathbf{y}}_j = [\hat{y}_1, \dots, \hat{y}_C] \in \{0, 1\}^C$  be the pseudo-labels for  $\mathbf{X}_j$  obtained by using a 0.5 threshold on the models

output probabilities  $\mathcal{F}(\mathbf{X}_j)$ . The approximation of the gradient embeddings with respect to the penultimate layer of  $\mathcal{F}$  for the loss  $\mathcal{L}_{BCE}$  is given by

$$g_{\mathbf{X}_j}^{\hat{\mathbf{y}}_j} = \nabla_W \mathcal{L}_{BCE}(\mathcal{F}(\mathbf{X}_j), \hat{\mathbf{y}}_j) \quad (6)$$

where  $W$  are the weights of the last layer of  $\mathcal{F}$ . For all unlabeled samples we compute the gradient approximation and measure its magnitude to obtain an estimation for the magnitude of the real loss gradient, which as stated before can be used to assess the sample's uncertainty. Consequently, the multi-label uncertainty of a sample based on the magnitude of approximated gradient embeddings is given by

$$Unc^{MGE}(\mathbf{X}_j) = \|g_{\mathbf{X}_j}^{\hat{\mathbf{y}}_j}\|_2. \quad (7)$$

### B. Evaluation of Multi-Label Diversity

For assessing the diversity of samples, we exploit a clustering-based approach. Clustering has been found an effective way to evaluate the diversity of samples in semantic segmentation and single-label scene classification problems in RS [10], since unlabeled uncertain images from different clusters are implicitly sparse in the feature space. We adapted this approach for assessing multi-label diversity. To this end, the  $m$  most uncertain samples (which are selected using one of the above-mentioned strategies to measure the multi-label uncertainty) are clustered into  $b$  clusters by using the Kmeans++ algorithm. Then, from each cluster we select the sample associated to the highest multi-label uncertainty, resulting in  $b$  selected samples. Due to selection of one sample from each cluster, the multi-label diversity of samples at each AL iteration is achieved.

We combine each multi-label uncertainty strategy with the clustering based multi-label diversity strategy. Accordingly, three query functions are investigated in this paper: 1) LL with Clustering (denoted by LL+Clustering), 2) TBD with Clustering (denoted by TPD+Clustering), 3) MGE with Clustering (denoted by MGE+Clustering).

## III. EXPERIMENTAL RESULTS

### A. Dataset Description and Design of Experiments

Experiments were conducted on the UCMerced [11] and TreeSatAI [12] datasets. The UCMerced dataset consists of 2100 RGB images, each of size  $256 \times 256$  pixels with 30cm spatial resolution. The total number of classes for this dataset is 17, while the number of labels associated with each image varies between 1 and 8 [1]. The images (i.e., samples) were randomly divided to derive a validation set of 525 samples, a test set of 525 samples, and a pool of 1050 samples. From the pool 40 images are randomly chosen as initial training samples and the rest are considered as unlabeled samples. The TreeSatAI dataset is made up of 50381 aerial images, each of size  $302 \times 302$  pixels containing RGB and near infrared bands. The total number of classes (corresponding to different tree species) for this dataset is 15, while the number of labels associated with each image varies between 1 and 6. The dataset contains information about area coverage ratio per label. For each class label, we compared its coverage ratio with

a threshold value and retained the label if the coverage ratio is higher than the threshold value. The value of the threshold is set to 0.07. This was resulted in the derivation of a validation set of 6799 samples, a test set of 5043 samples, and a pool of 38531 samples. The images were resized to  $288 \times 288$  pixels to tailor them to the model. From the pool 1000 images are randomly chosen as initial training samples and the rest are considered as unlabeled samples.

We report our results in terms of  $F_1$  scores. All experimental results are referred to the average accuracies obtained in three trials according to three initial randomly selected training sets. We used Densenet121 [13] as the DL model  $\mathcal{F}$ . For training we utilized the SGD optimizer with an initial learning rate of 0.025 on UCMerced and 0.01 on TreeSatAI. For UCMerced, we trained the model for 100 epochs using a batch size of 10. For TreeSatAI, we train for 200 epochs using a batch size of 100. We reduce the learning rate by a factor of 0.1 after 80 epochs on UCMerced and after 160 on TreeSatAI. We apply simple data augmentation techniques including horizontal flipping and random rotation of  $r \in \{0, 90, 180, 270\}$  degrees. For UCMerced we set  $m = 3$ , while for TreeSatAI we set  $m = 4$ . For LL, we empirically found  $\lambda = 0.1$  to provide good results and set  $\xi = 1$  as suggested in [7]. For the auxiliary loss prediction module, we used Adam optimizer with the same initial learning rate as for the DL model optimizer and stop gradient propagation to the DL model after 60th epoch for UCMerced and after 120th epoch for TreeSatAI as suggested in [7]. The model training and further experiments were conducted on a NVIDIA A100 GPU with 82 GB RAM.

### B. Sensitivity Analysis

In this subsection, we initially analyse the performances under different values of the labeling budget  $b$  by fixing the query function. Figure 1 shows the  $F_1$  scores versus the number of training samples using the LL+Clustering query function for the UCMerced dataset. From the figure, one can observe that selecting small  $b$  values results in higher  $F_1$  scores under the same number of labeled samples. Furthermore, in the case of using small  $b$  values higher  $F_1$  scores are achieved with less samples compared to the cases of larger  $b$  values. However, since at each AL iteration the DL model has to be trained on all the labeled samples, small  $b$  values are associated to the higher training complexity. Note that similar behaviors are obtained with the other query functions applied to both datasets (not provided due to space limitations). We also analyse the accuracy obtained by using only multi-label uncertainty criterion and also its combination with multi-label diversity criterion. Figure 2 shows the average  $F_1$  scores versus the number of training samples obtained by LL ( $m$  is fixed equal to  $b$ ) and LL+Clustering when  $b=20$  for the UCMerced dataset. By analysing the figure one can observe that as expected the classification performances are significantly improved by using both uncertainty and diversity criteria under each number of labeled samples. These results are also confirmed in other experiments with the other query functions applied to both datasets (not reported for space constraints).

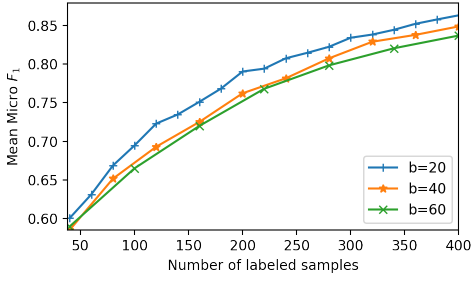


Fig. 1:  $F_1$  scores versus the number of training samples obtained by LL+Clustering with different  $b$  values (UCMerced dataset).

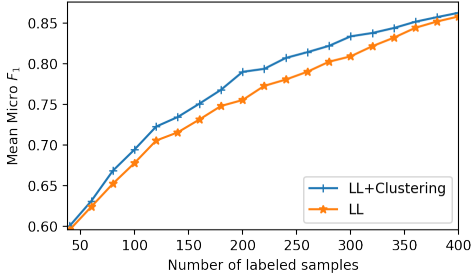


Fig. 2:  $F_1$  scores versus the number of training samples obtained by using LL and LL+Clustering when  $b=10$  (UCMerced dataset).

The last analysis of this sub-section is associated to the initialisation of the model parameters. There are two different strategies for initialising the model parameters at each AL iteration: 1) random initialisation that is associated to cold-starting; and 2) using the parameters learned in the previous AL iteration (except in the first iteration where the initialisation is random) that is associated to warm-starting. We analysed the effect of the two initialisation strategies on the model performance. Figure 3 shows the mean  $F_1$  scores for LL+Clustering on UCMerced and TreeSatAI using warm-starting and cold-starting. From the figure, we can see that using warm-starting results in higher scores on the UCMerced dataset (Fig. 3a). In the first few iterations the model achieves already quite good performance, which means that the learned weights already capture valuable knowledge about the data. Therefore, the model can benefit from re-initialising with previously learned weights. However, for TreeSatAI the figure shows that cold-starting leads to a better overall performance (Fig. 3b). In addition, at the first iterations warm-starting shows no benefit, whereas during subsequent iterations, when the model already achieves relatively good results, there are minor benefits. However, at later iterations warm-starting causes the model to over-fit, such that performance is stagnating. This is caused by the accumulation of network updates over the course of the AL iterations.

### C. Comparison Among the Investigated Query Functions

In this section we compare our query functions (LL+Clustering, TPD+Clustering, MGE+Clustering) among each other and with random sampling in terms

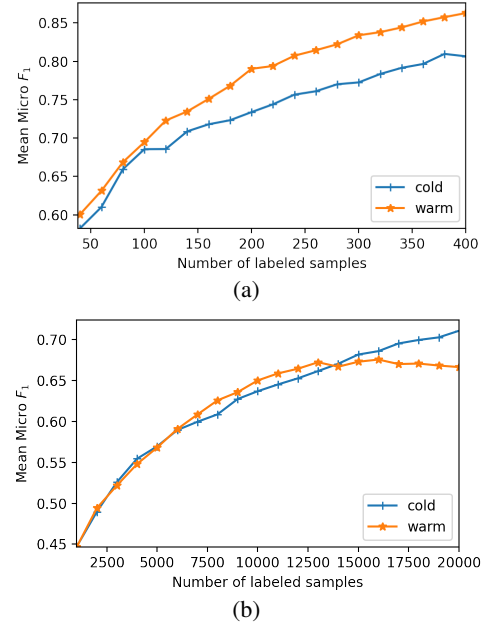


Fig. 3: Results for LL+Clustering in terms of micro  $F_1$  score using cold-starting and warm-starting on (a) UCMerced; and (b) TreeSatAI.

of classification accuracy and complexity (associated to the trainable parameters and time needed for sampling). Figure 4 shows the micro  $F_1$  versus the number of labeled samples for the UCMerced dataset using warm-starting. From the figure we can see that all our query functions provide similar performances. However, in general MGE+Clustering results in slightly higher micro  $F_1$  scores. In addition, our query functions outperform random sampling particularly at the later AL iterations. As an example, MGE+Clustering outperforms random sampling by more than 2% reaching a micro  $F_1$  score of 79.87% with 200 labeled samples, and more than 1% reaching a micro  $F_1$  score of 85.81% with 400 labeled samples. As an other example, LL+Clustering outperforms random sampling by more than 1% with a micro  $F_1$  score of 86.29% at 400 labeled samples. We have found similar results in terms of macro  $F_1$  score but could not report for space constraints. Figure 5 shows the  $F_1$  scores versus the number of training samples obtained for TreeSatAI using cold-starting. From the figure we can see that the three query functions show similar performance, clearly outperforming random sampling in terms of micro  $F_1$  score (Fig. 5a). For example, reaching 69.90% LL+Clustering outperforms random sampling by more than 2% with 18000 labeled samples. From figure 5b we can see that LL+Clustering provides the best macro  $F_1$  scores. LL+Clustering outperforms random sampling by 8% reaching a macro  $F_1$  score of 59.05% with 14000 labeled samples. MGE+Clustering outperforms random sampling by about 5% with 14000 labeled samples reaching a macro  $F_1$  scores of 55.49% and TPD+Clustering outperforms random sampling by more than 4% reaching a macro  $F_1$  score of 54.74%. Table I shows the sampling time and the number of trainable parameters for each method. LL+Clustering

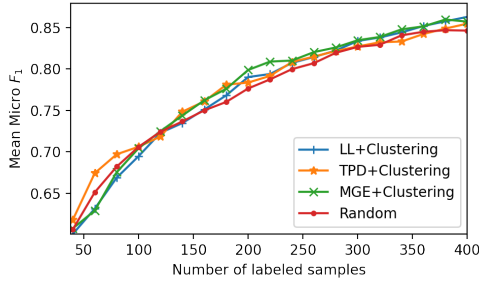


Fig. 4: Micro  $F_1$  scores versus the number of labeled samples obtained by our query functions and random sampling using warm-starting (UCMerced dataset).

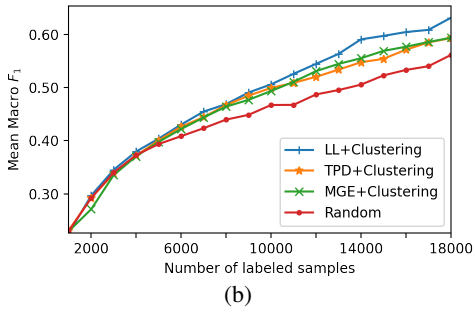
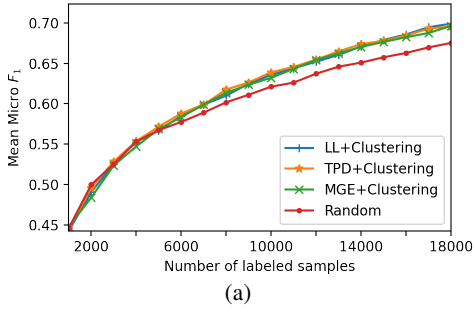


Fig. 5: (a) Micro  $F_1$  and (b) macro  $F_1$  scores versus the number of labeled samples obtained by our query functions and random sampling using cold-starting (TreeSatAI dataset).

has the highest number of trainable parameters as well as hyper-parameters, which may require some additional effort for tuning. The time for selecting the most informative samples at one AL iteration are similar for LL+Clustering and MGE+Clustering, whereas TPD+Clustering is slightly slower due to the computation overhead of the reference model.

#### IV. CONCLUSION

In this letter, we have investigated three different AL query functions in the framework of DNNs for the MLC of RS

TABLE I: Time needed for selecting  $b$  unlabeled samples and the number of trainable parameters for each AL method.

Method	UCMerced ( $b=20$ )	TreeSatAI ( $b=1000$ )	Parameters
LL + Clustering	7.25s	141.5s	7.33M
TPD + Clustering	10.84s	188.1s	6.97M
MGE + Clustering	7.06s	142.2s	6.97M

images. The presented query functions are based on the evaluation of two criteria: i) multi-label uncertainty; and ii) multi-label diversity. To evaluate multi-label uncertainty, we have presented and adapted to MLC problems three different strategies: i) learning multi-label loss ordering; ii) measuring temporal discrepancy of multi-label prediction; and iii) measuring magnitude of approximated gradient embedding. To achieve multi-label diversity, we have exploited a clustering based strategy. We have combined each multi-uncertainty evaluation strategy with the clustering based strategy, resulting in three different query functions. It is worth emphasizing that our query functions are independent from the considered DL model and can be embedded within any DL model designed for MLC problems. From the experiments conducted on two multi-label benchmark datasets, we have observed that the combination of learning multi-label loss ordering with clustering leads to the best overall performance, whereas that of measuring magnitude of approximated gradient embedding is computationally more efficient with a slight decrease in the accuracy. As a future work, we plan to adapt and test our query functions in the framework of multi-label RS image retrieval problems.

#### REFERENCES

- [1] B. Chaudhuri, B. Demir, S. Chaudhuri, and L. Bruzzone, "Multilabel remote sensing image retrieval using a semisupervised graph-theoretic method," *IEEE Transactions on Geoscience and Remote Sensing*, vol. 56, no. 2, pp. 1144–1158, 2018.
- [2] B. T. Zegeye and B. Demir, "A novel active learning technique for multi-label remote sensing image scene classification," in *Image and Signal Processing for Remote Sensing XXIV*, vol. 10789, 2018, pp. 100–107.
- [3] R. Thoreau, V. Achard, L. Risser, B. Berthelot, and X. Briottet, "Active learning for hyperspectral image classification: A comparative review," *IEEE Geoscience and Remote Sensing Magazine*, vol. 10, no. 3, pp. 256–278, 2022.
- [4] G. Lenczner, A. Chan-Hon-Tong, B. Le Saux, N. Luminari, and G. Le Besnerais, "Dial: Deep interactive and active learning for semantic segmentation in remote sensing," *IEEE Journal of Selected Topics in Applied Earth Observations and Remote Sensing*, vol. 15, pp. 3376–3389, 2022.
- [5] S. Sinha, S. Ebrahimi, and T. Darrell, "Variational adversarial active learning," in *IEEE/CVF International Conference on Computer Vision*, 2019, pp. 5971–5980.
- [6] K. Kim, D. Park, K. I. Kim, and S. Y. Chun, "Task-aware variational adversarial active learning," in *IEEE/CVF Conference on Computer Vision and Pattern Recognition*, 2021, pp. 8162–8171.
- [7] D. Yoo and I. S. Kweon, "Learning loss for active learning," in *IEEE/CVF Conference on Computer Vision and Pattern Recognition*, June 2019.
- [8] S. Huang, T. Wang, H. Xiong, J. Huan, and D. Dou, "Semi-supervised active learning with temporal output discrepancy," in *IEEE/CVF International Conference on Computer Vision*, October 2021, pp. 3447–3456.
- [9] J. T. Ash, C. Zhang, A. Krishnamurthy, J. Langford, and A. Agarwal, "Deep batch active learning by diverse, uncertain gradient lower bounds," *arXiv:1906.03671*, 2019.
- [10] B. Demir, C. Persello, and L. Bruzzone, "Batch-mode active-learning methods for the interactive classification of remote sensing images," *IEEE Transactions on Geoscience and Remote Sensing*, vol. 49, no. 3, pp. 1014–1031, 2011.
- [11] Y. Yang and S. Newsam, "Geographic image retrieval using local invariant features," *IEEE Transactions on Geoscience and Remote Sensing*, vol. 51, no. 2, pp. 818–832, 2013.
- [12] S. Ahlswede, C. Schulz, C. Gava, P. Helber, B. Bischke, M. Förster, F. Arias, J. Hees, B. Demir, and B. Kleinschmit, "Treesatai benchmark archive: A multi-sensor, multi-label dataset for tree species classification in remote sensing," *Earth Syst. Sci. Data Discuss.*, 2022.
- [13] G. Huang, Z. Liu, L. van der Maaten, and K. Q. Weinberger, "Densely connected convolutional networks," in *IEEE Conference on Computer Vision and Pattern Recognition*, July 2017.